IEEE Photonics Journal
An IEEE Photonics Society Publication

Open Access

LED-Based Collimating Line-Light Combining Freeform and Fresnel Optics

Volume 10, Number 6, December 2018

AnneMarie McCarthy
Javier Romero-Vivas
Ciara O'Hara
Natalia Rebrova
Liam Lewis
Stephen P. Hegarty

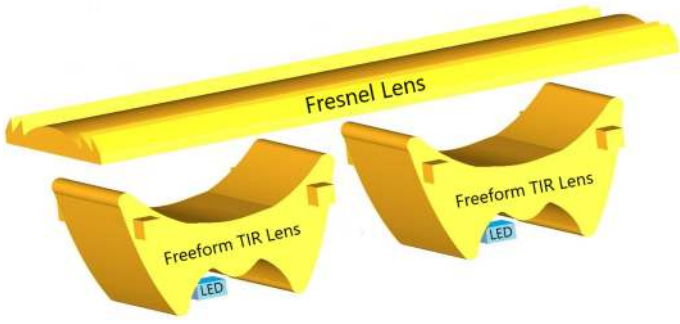

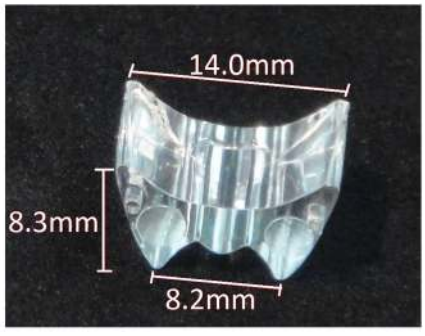

DOI: 10.1109/JPHOT.2018.2876381
1943-0655 © 2018 CCBY

IEEE photonics SOCIETY

IEEE

LED-Based Collimating Line-Light Combining Freeform and Fresnel Optics

AnneMarie McCarthy,[1] **Javier Romero-Vivas**,[2] **Ciara O'Hara**,[1,3] **Natalia Rebrova**,[1,4] **Liam Lewis**,[1,4] **and Stephen P. Hegarty**[1,4]

[1]Cork Institute of Technology, Cork T12 P928, Ireland
[2]TQS Integration, Ltd., Waterford P51 H01X, Ireland
[3]ProPhotonix, Ltd., Cork T45 X211, Ireland
[4]Tyndall National Institute, Cork T12 R5CP, Ireland

DOI:10.1109/JPHOT.2018.2876381
This work is licensed under a Creative Commons Attribution 3.0 License. For more information, see http://creativecommons.org/licenses/by/3.0/

Manuscript received April 24, 2018; revised October 9, 2018; accepted October 12, 2018. Date of publication October 16, 2018; date of current version October 30, 2018. This work was supported in part by the European Community through the FP7 "Research for SMEs" Project NISTAS under Contract 606668 and in part by the Irish Research Council. Corresponding author: AnneMarie McCarthy (e-mail: annemarie.mccarthy@cit.ie).

Abstract: Illumination for line-scan machine vision systems is required to produce a highly asymmetric elliptical beam pattern, to maximize system speed and accuracy. The use of LED emitters with symmetric Lambertian emission patterns is challenging in this context, requiring significant beam reshaping. A design for a collimated line-light, with long working distance, utilizing LEDs with symmetric Lambertian emission patterns, is presented. Using a combination of Fresnel lenses and total internal reflection (TIR) optics, an elliptical beam with a high degree of collimation is achieved. TIR elements are designed based on an adaptation of a freeform lens design method published by Chen *et al.* [Opt. Express 20, 10 (2012)]. Practical performance of the design is verified experimentally using a prototype unit. In addition, the design is compared, using ray tracing software, to line-lights constructed using commercially available symmetric and elliptical TIR lenses, and its superior performance is confirmed. The optical design described is fully manufacturable and suitable for both small- and large-scale production.

Index Terms: LEDs, collimation, line-light, freeform optics, machine vision.

1. Introduction

Line based inspection, using linear image sensors, is a common tool used in machine vision technology, where non-destructive in-line inspection is required [1], [2], with machine vision inspection methods providing improvements over manual inspection generally [3]. It is particularly suited to applications requiring high speed web inspection, where the use of time-delay and integration techniques allows it to outperform standard single shot methods [4]. Examples of materials which can be inspected in this manner include PCBs, cotton, textiles, machined parts, paper, hot steel, silicon wafers and food produce [1], [2], [4]–[9]. Line-scan methods are also applicable to other inspection tasks, such as plate defect detection [10]. Using standard line-scan technology, web inspection can be performed at a rate on the order of meters per second, significantly outperforming manual inspection methods in speed, accuracy and resolution [11]. Lighting requirements for these systems are challenging, and in particular the irradiance of the lighting can be a rate limiting factor, due to the short exposure times. Ideally, to maximize signal to noise, the lighting should achieve a rectangular uniform high irradiance beam, concentrated on the field of view of the camera [12]. In

many applications, a minimum distance from the surface of interest to the illumination and sensor must also be maintained. This is often due to overall system mechanical constraints, but can also be due to issues such as risk of contamination (e.g., food industry), or damage to the sensor/lighting system (e.g., hot steel inspection [5]).

A laser line generator can be constructed using a cylindrical lens [13], [14], diffractive optics [15], a Powell lens [16], or a microlens array [17]. Although such construction leads to a simple and robust system, speckle arises when such a laser-line is projected onto a rough surface. The image obtained by the system camera will show time varying intensity patterns due to the superposition of rays which travel stochastically varying optical path-lengths. One possible strategy to avoid this is to replace laser based illumination with LED-based illumination. LEDs are devices with a much smaller spatial and temporal coherence than lasers and, consequently, LED light projected on rough surfaces exhibits no speckle. Additional features making the use of LEDs attractive are their longevity, low cost, reduced size, high radiant power, and electrical and optical performance [12], [18].

In order to produce a rectangular beam pattern, the symmetrical Lambertian emission pattern of an LED or LED array must be reshaped using secondary optics. The design of such a system is challenging. A possible approach is the use of a microlens array which can shape and also diffuse and/or homogenise the beam. [19], [20]. These systems can be highly effective for some applications. However, the limited power output from a single LED package, combined with the relatively high cost of microlens array optics, makes this strategy prohibitively expensive for many line-scan machine vision applications, where the web inspection area can be many metres in width [21]. An alternative cost-effective approach followed by many commercial manufacturers is the use of a linear LED array coupled to an array of commercially available TIR lenses (See Section 4). However, this approach is inherently inefficient, providing relatively low irradiance at the target plane. More optically efficient designs, based on free-form lenses, have also been proposed [13], [22]–[24]. For example, a freeform secondary optics design based on the use of two cylindrical spherical lenses, producing a rectangular beam for a street-lighting application [13]. However, in general the fabrication of freeform designs can be complicated and incur significant cost. In addition, many machine vision illumination system manufacturers prefer flexibility in the system design, with the ability to produce linear beam patterns of easily customizable width, suitable for multiple applications, with varying camera fields of view. Use of freeform lenses which produce application specific beam patterns then poses a practical problem, as different unique lens designs, and hence a different molding process (with the associated cost of same) is required for each new application.

In this paper, a method is proposed for LED line-light collimation and beam shaping, involving control of the LED radiation pattern in orthogonal axes, parallel and perpendicular to a linear LED array.

2. Optical Design of the System

Typical line-scan setups have fields of view (FOV) of the order of 100 mm $\times$ 100 μm ($\sim$20° $\times$ 0.02° at 300 mm working distance) [4]. To maximize irradiance on the field of view, the ideal illumination pattern is then rectangular in nature. In the long axis, the optimal beam divergence of the optical system should not exceed the camera angular FOV ($\sim$20° at 300 mm).

As the physical size of the LED emitting aperture (typically $>$200–300 um [25]) exceeds the short axis FOV of the line scan setup (100 μm at 300 mm [4]), the required magnification (i.e., image size/object size or desired beam size/LED emitting aperture size) in this axis is $<$1, for optimal illumination. For example, using a 300 μm chip on board LED, a magnification of 100 μm/300 μm $=$ 0.33 is required. Such low magnification can be achieved (with physically small LEDs) at short working distances (typically $<$50 mm), through the use of a low focal length lens, and this arrangement is practical for many machine vision tasks. However, where larger distances must be maintained between the illumination and the target area, a more challenging scenario presents. In this case, low magnification ($<$1) is not practical, being limited by the permitted mechanical size of

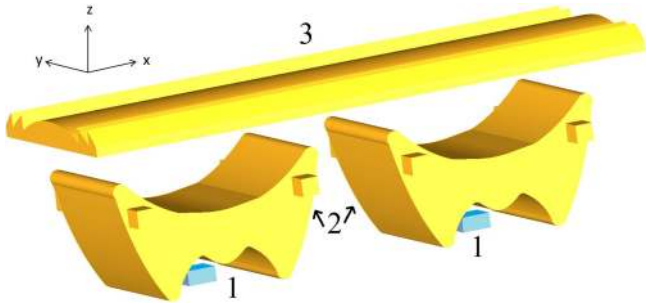

Fig. 1. Concept of the proposed optical system. The cubes (1) depict the LEDs. An array of custom-made lenses (2) collimate the light in the x-direction (primary lenses). A Fresnel lens (3) above collimates the rays in the y-direction (secondary lens).

the illumination system, and the width of the illumination beam pattern will, necessarily, be larger than the FOV of the line scan camera. When the working distance (from system optics to target plane) significantly exceeds (typically $>$500 mm) the distance from the source LEDs to the system optics, optimal illumination of the target area is achieved through collimation of the light source in the short axis. The optical system was designed to achieve such collimation, with optimal results achieved for working distances $>$500 mm. However, it should be noted, that the resultant system is easily configurable for shorter ($<$500 mm) working distances, and customizable beam width (in the short axis), through the simple replacement of the Fresnel lens element, with a lens of shorter focal length.

In a system utilizing a simple array of LEDs and symmetric collimating lenses (e.g., see Section 4, Carclo lenses), the diameter of the lensing elements is limited by the LED pitch. However, according to the principle of conservation of étendue [27], to achieve maximum collimation in the short axis of the optical system, the entrance pupil of the optical system in the short axis should be maximized. Ideally, it should be limited only by the overall mechanical constraints of the system. The simplest method of achieving this practically is a dual lensing arrangement, as illustrated in Fig. 1, with the lensing in the short axis (y-axis) provided by a single cylindrical surface (Fig. 1, element 3). Cylindrical lenses of this type are readily available commercially, most practically in the form of Fresnel lenses, which compact the lens design into a thinner profile. Adopting this strategy, the design can incorporate a secondary lens with a lens diameter (and hence focal length) restricted only by the overall mechanical constraints of the system, and not by the LED pitch.

The primary lenses (Fig. 1, element 2) consist of custom-made TIR elements which collimate the output of each individual LED in the long axis (x-axis). These are designed using a freeform method for TIR construction published in Chen *et al*. [26]. Such methodology follows a set of strategies based on combinations of refraction and reflection to re-direct light from the LEDs to a direction perpendicular to the plane of the PCB holding the LEDs, as shown in Fig. 2. As a stable and firm support was required for the TIR elements it was decided to implement only the strategies using ray groups 1 and 2. The edge of the lens was modified, as shown in Fig. 3, to provide a bigger contact area with the support. The overall efficiency of the lens (implementing only ray groups 1 and 2) was estimated by optical modelling as 64% (based on an optical system with f# of 0.5. More details on the methodology employed are provided in Section 3.2), or equivalently a loss of 36% of optical power is observed. Of the total 36% optical loss, the decision to not implement ray group 3 accounts for less than 10%.

A MATLAB software algorithm based on Snell's law was developed to implement the functionality of ray groups 1 and 2 with an idealized point source, while accounting for the optical properties of the material (Polymethyl methacrylate or PMMA). The profile obtained is shown in Fig. 3(a). As the purpose of this study was to use the TIR for collimation in a single axis only, it was decided to extrude the profile out of the plane. The resulting TIR lens design was manufactured by Proto Labs, Ltd., UK, using injection molding of PMMA. To accommodate the manufacturing process, a

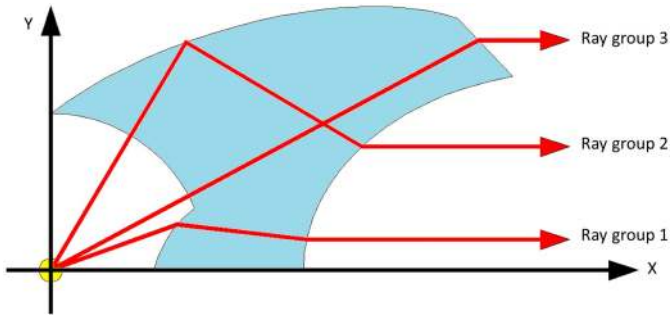

Fig. 2. Ray diagram showing the 3 different working areas of the TIR proposed by Chen *et al.* [26]. Point source located at the origin. Ray group 1: double refraction. Ray group 2: Refraction + reflection + refraction. Ray group 3: double refraction.

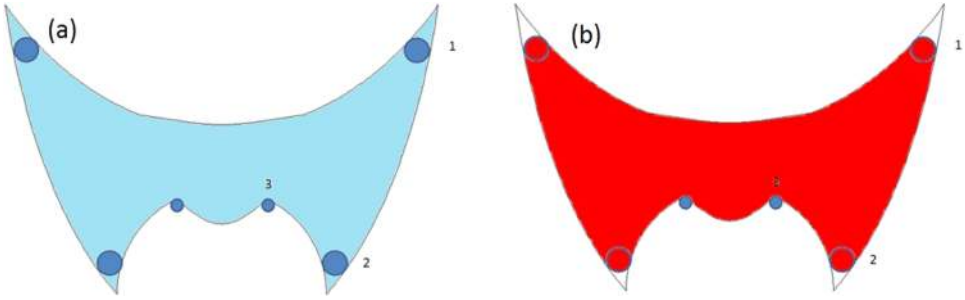

Fig. 3. (a) Initial design of a primary lens element. This design is not suitable for fabrication by molding. The numbered points indicate areas where fill problems can occur during the molding process. To correct this, a minimum radius was applied to areas where 'sharp corners' occur. The final design, shown in (b) is suitable for manufacture by injection molding.

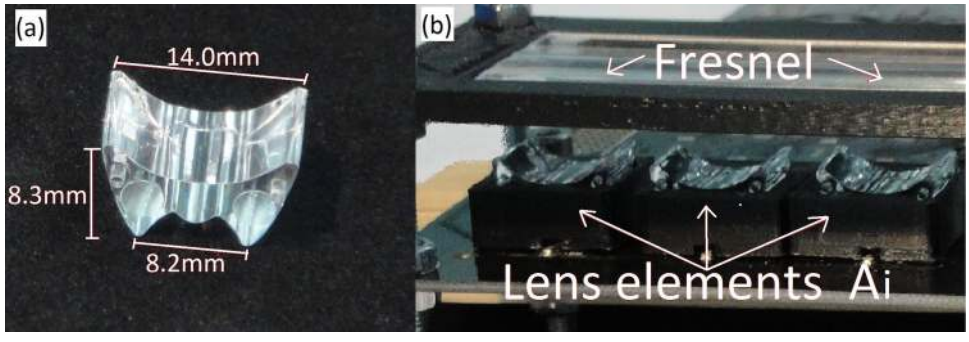

Fig. 4. (a) Fabricated single primary lens element A_i (b) Complete optical system including primary lens elements in lens-holders, and secondary Fresnel lens.

number of minor design alterations were necessary (see Fig. 3(b)). In particular, in consultation with the manufacturer, areas of the design which resulted in extreme thinness or 'sharp corners' were removed to improve material flow, and to enable successful removal from the mold.

A single fabricated primary lens, and a cross-section of the complete linear optical design, incorporating both primary lens elements A_1–A_n (where n is the number of LEDs), and secondary (Fresnel) lens, are shown in Fig 4. The design, as shown, is cost effective and suitable for large volume fabrication. A further simplification in the design could be achieved by placing the Fresnel lens pattern on the front surface of the primary lens elements, effectively combining the Fresnel

and primary lens elements. However, this would fix the beam width and working distance of the unit, requiring a remolding of new primary lens elements for any applications requiring an alternative beam width or working distance. As the parameters and working conditions of linescan web inspection applications are so widely variable, it was decided to keep a degree of flexibility in the linelight design. The chosen design allows for the production of customizable beam widths, and choice of working distance, via the replacement or movement of just the Fresnel element.

3. Optical Modeling and Experimental Results

3.1 Experimental and Optical Modeling Details

All optical modeling was completed using Zemax 13 [28] (non-sequential mode), with ray tracing performed using 1 million rays per LED. Zemax is a powerful ray tracing software tool allowing the user to simulate a variety of experimental optical systems and assess changes to the system without the need for full experimental iterations. The Osram Mini TOPLED model utilized manufacturer assembled ray-set files which are provided for optical modeling purposes and which describe the spatial and angular luminance characteristics of the source. Where appropriate, results were smoothed (smoothing parameter $= 5$) to reduce noise in the data. Each LED was assigned a radiometric power of 1 W (except in Section 4, where the array power was instead fixed), to allow for convenient assessment and comparison of results. It should however be noted that the powers of the LED types modeled are typically less than 1 W, with the OSRAM Mini TOPLED (blue), having a typical output power of approx. 1.2–4.8 mW (based on a typical luminous intensity of 22.4–90 mCd), while the Duris E2, based on a luminous flux of 25.5 lm, has a typical output power of approx. 100–150 mW (dependent on drive current, binning, substrate temperature and other factors).

Experimentally, beam profiles were measured using a photodiode array (TAOS TSL1412S), with 65 μm resolution. The full optical system, which was tested experimentally, comprised eight OSRAM Mini TOPLED LEDs (blue) (product code LB M673) in a linear array, with pitch (LED spacing) of 15 mm. Monochromatic sources were selected as the photodiode array has a limited spectral response, impairing its ability to correctly measure irradiance of broadband sources. Lens elements were centered and placed using the lens holders (one LED per TIR lens) shown in Fig. 4(b). The Fresnel lens selected for test was obtained from Edmund Optics (#46-110, EFL 19.05 mm, Effective Size 19.05 $\times$ 302.26 mm). In all cases, the term 'working distance' refers to the distance from the measurement plane to the element of the optical system which lies farthest from the LED(s). Mechanical axes *x* and *y* in the system are as defined in Fig. 1.

3.2 Lensing Elements A_n

To assess the performance of the manufactured lenses, an experimental setup was built comprising a single LED (OSRAM Mini TOPLED) and lens element A_n. This system was measured via photodiode array at a variety of working distances by plotting the relative optical power at the fixed distance versus the horizontal distance from the center of the system. Measurements were made parallel to the long axis of the lens element A_n i.e., in the axis of collimation (Mechanical axis *x,* see Fig. 1). In addition we have also included the theoretically modeled output of the same optical system using the Zemax modeling tool. The experimental results are seen to agree well with the ray tracing results, as shown in Figs. 5 and 6, producing similar line profiles and line-widths. Some discrepancies are observed as the distance from the lens increases. This can, in part, be attributed to a mechanical tolerance which applies in the placement of the lens with respect to the LED. Tolerances derived from the molding process must also be considered as potential contributors to the observed discrepancies. In general, however, the manufactured and assembled lenses were observed to perform very similarly to the optically modeled lenses.

The high level of accuracy achieved by the model in recreating the experimentally observed beam shape, gives a high level of confidence in the model's ability to accurately characterize the

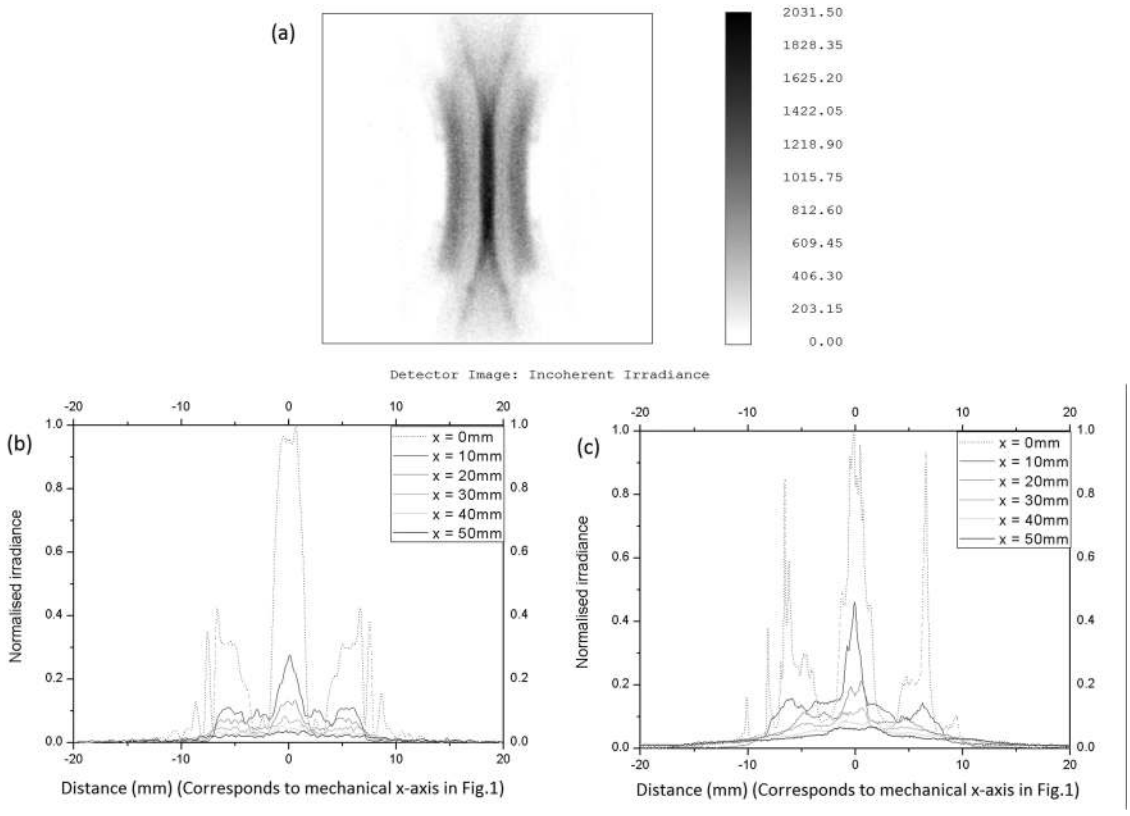

Fig. 5. (a) Optical modeling of irradiance distribution from a primary lens element A_n at a working distance of 25 mm. Detector size 50 $\times$ 50 mm. Source power $=$ 1 W. Power at detector $=$ 0.64 W, (b) Optically modeled and (c) Experimentally measured beam profiles achieved at various working distances, using a single primary lens element A_n. (In (a), the y-axis corresponds to the mechanical y-axis (See Fig. 1)).

optical surfaces of the TIR lenses, and estimate optical parameters of the system such as angular divergence and efficiency. Section 3.3 shows that the same can be said for the optical model of the line-light design as a whole.

Angular divergence and efficiency of the lens design was assessed using optical modeling. Using a planar detector of size 50 $\times$ 50 mm, placed at a working distance of 25 mm (equivalent to an optical system with f# $=$ 0.5), an efficiency of 64% is achieved (Fig 5a). The primary factor which compromises the optical efficiency of the lensing elements is the presence of the two planar surfaces, present due to extruding the profile to provide collimation in one axis only. Some control is achieved in the short axis, due to the presence of the refractive surfaces, but optical power is also lost to total internal reflection at these surfaces. The overall angular divergence of the beam (measured on a polar detector at 500 mm working distance), is $\sim 7^\circ \times 50^\circ$ (Axes $x \times y$), compared to an angular divergence of $120^\circ \times 120^\circ$ (i.e., Lambertian emission), for the LED alone. In comparison, the angular divergence of the beam measured using the same detector is $\sim 5^\circ \times 33^\circ$ (Axes $x \times y$) when a point source is used as the source.

3.3 Full Optical System

A prototype of the full optical system described in Section 3.1 was assembled. Fig. 7 shows the results of an experimental test of the fully assembled system (with Fresnel lens of focal length 19 mm), alongside the results of ray tracing of the same optical system. Beam profiles in the axis

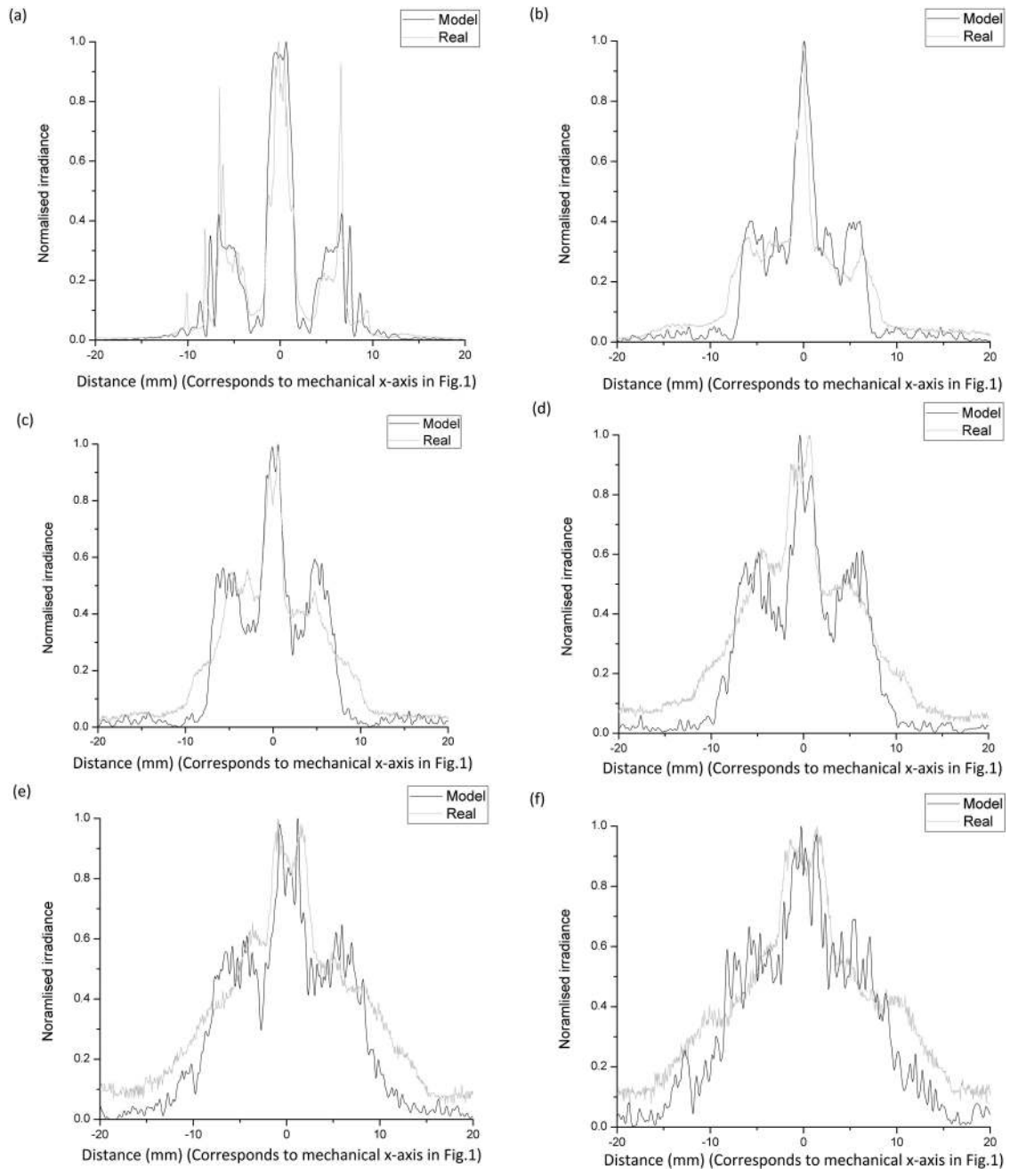

Fig. 6. Normalised optically modeled and experimentally measured beam profiles measured at working distances of (a) 0 mm, (b) 10 mm, (c) 20 mm, (d) 30 mm, (e) 40 mm, and (f) 50 mm using a single primary lens element A_n.

perpendicular to the linear array (Mechanical axis *y,* See Fig. 1) were obtained experimentally, at working distances of 500 mm and 1000 mm. Good agreement is observed between the experimental and simulated results, with the optical model predicting the general beam-profile and beam-width quite accurately. A beam divergence of $\sim 2^\circ$ is observed experimentally. Discrepancies observed between modeled and experimental results may be attributable in part to the use of the object type 'Fresnel 2' in Zemax 13, which models the Fresnel lens using the approximation that the Fresnel faces are infinitesimally small. The object type Fresnel 1 allows more detailed modeling of specific

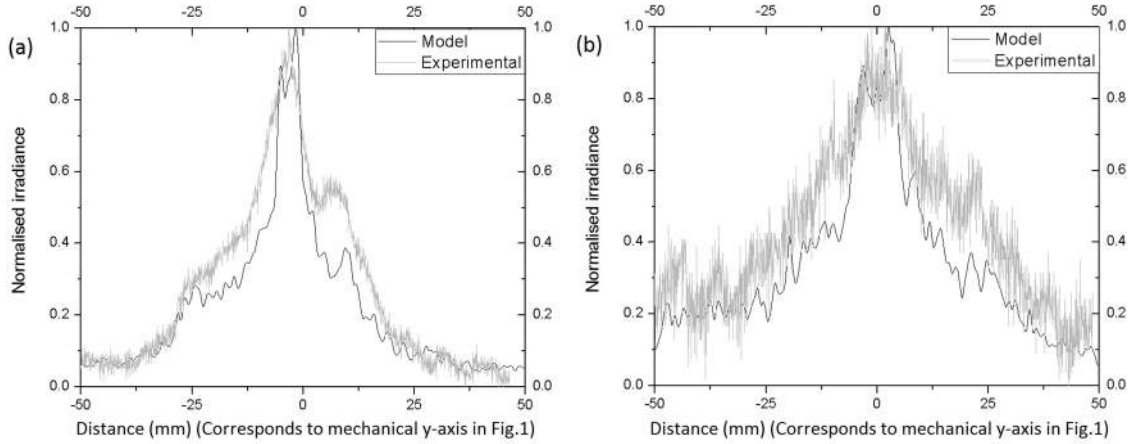

Fig. 7. Optically modeled and experimentally measured beam profiles achieved using the proposed optical system (Primary lens elements: A_n; Secondary lens: Fresnel lens (efl = 19 mm)) at working distances of (a) 500 mm, (b) 1 m.

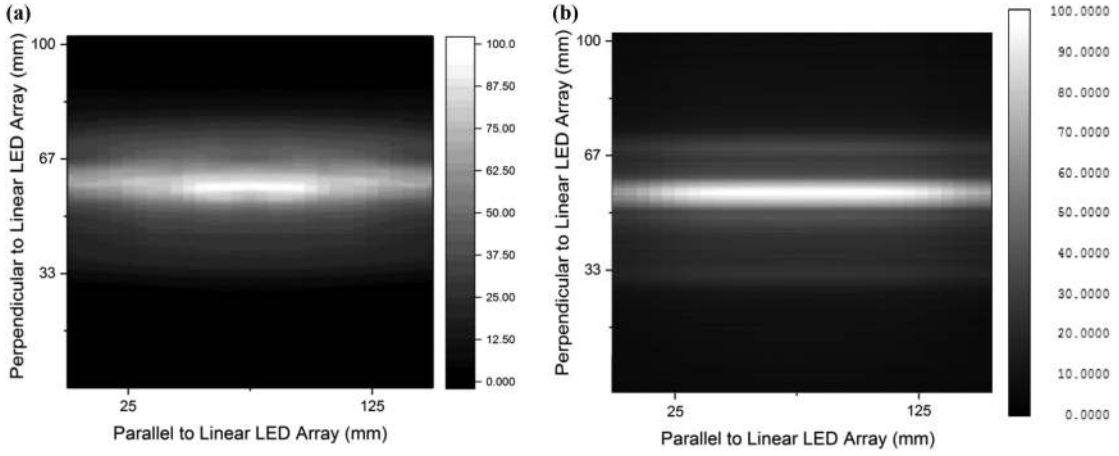

Fig. 8. (a) Experimentally measured and (b) Optically modeled grayscale irradiance maps of normalized beam profiles at working distance 500 mm, for full optical system (Primary lens elements: A_n; Secondary lens: Fresnel lens (efl = 19 mm). Detector size for (b) is 150 × 100 mm (i.e., equivalent to scale of experimental plot). (The x and y axes correspond to the mechanical x and y axes (See Fig. 1)).

Fresnel surface types, but requires additional computational time, and an exact knowledge of the Fresnel surface (e.g., groove pitch, depth, frequency), which was not available in the case of the lens used in this experiment.

Fig. 8 shows the results of an experimentally measured and optically modeled mapping of the full beam profiles at a working distance of 500 mm. Beam profiles in the axis perpendicular to the linear array, (Mechanical axis y, See Fig. 1), each 100 mm in length, were measured across 150 mm (measured parallel to the linear LED array, Mechanical axis x in Fig. 1) of the beam length. Profiles obtained were assembled in a grayscale color map. The optical model was adjusted to achieve equivalent resolution to the experimental system. An overall beam divergence of $\sim 2^\circ \times 18^\circ$ (see Fig. 1, Mechanical axes y × x) is observed experimentally. Of particular interest is the asymmetry of the beam, which is observed in both the experimental and modeled data, in Figs. 9 and 10. This is a feature of the OSRAM Mini TOPLED, which is reproduced both experimentally, and in the manufacturer assembled ray-set files. The impressive agreement between experiment and model serves to increase confidence in the optical model results.

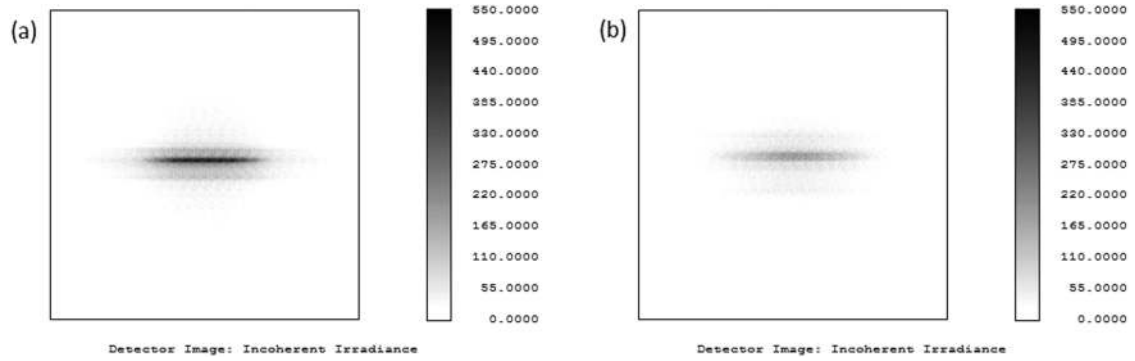

Fig. 9. Optical modeling of the proposed optical system. (Primary lens elements: A_n; Secondary lens: Fresnel lens (efl = 19 mm)). Detector size: 400 × 400 mm. Greyscale represents incoherent irradiance (Wm^{-2}) (a) Results of ray-tracing procedure at a working distance of 500 mm, Max. Irradiance = 455 Wm^{-2} (b) Results of ray tracing procedure at a working distance of 1 m, Max. Irradiance = 190 Wm^{-2}. (The x and y axes correspond to the mechanical x and y axes (See Fig. 1)).

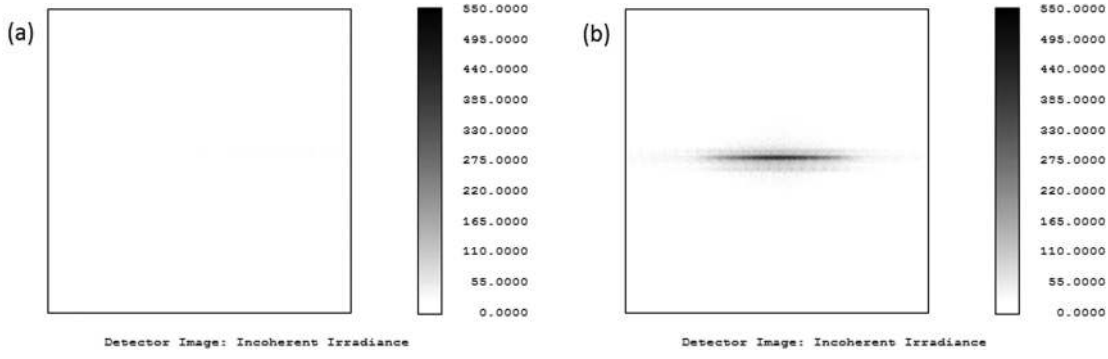

Fig. 10. Results of optical modeling (at 1 m working distance) (Detector size: 400 × 400 mm .Greyscale represents incoherent irradiance (Wm^{-2})) with (a) Primary lens elements: none; Secondary lens: Fresnel lens (efl = 19 mm) Max. Irradiance = 20 Wm^{-2} (b) Primary lens elements: A_n; Secondary lens: Fresnel lens (efl = 50 mm). Max. Irradiance = 405 Wm^{-2}. (The x and y axes correspond to the mechanical x and y axes (See Fig. 1)).

Further optical modeling of the system was completed to demonstrate the characteristics of the optical system. In Fig. 9, beam profiles at working distances of 500 mm and 1 m are shown, demonstrating the change in beam profile and irradiance with increased working distance. In Fig. 10, the optical design was altered to demonstrate the action of the primary and secondary lens elements. Removal of the primary lens elements A_n from the design was seen to lead to a 90% reduction in beam irradiance (Fig. 10a versus Fig. 9b). An increase in focal length (and diameter) of the secondary lens to 50 mm (from 19 mm) resulted in a 113% increase in peak beam irradiance (Fig. 10b versus Fig. 9b). This trend is as expected, arising from the increase in beam area or size, and concurrent reduction in radiating solid angle of the beam (or increased collimation).

4. Comparison to Commercially Available Solutions

An alternative method of constructing a collimating line-light is the use solely of a linear array of commercially available TIR lenses. These lenses are designed using the same principles used for the design of the primary lens elements A_n; a heuristic approach based on the splitting of the available volume in regions where using a combination of refraction and reflection, the desired

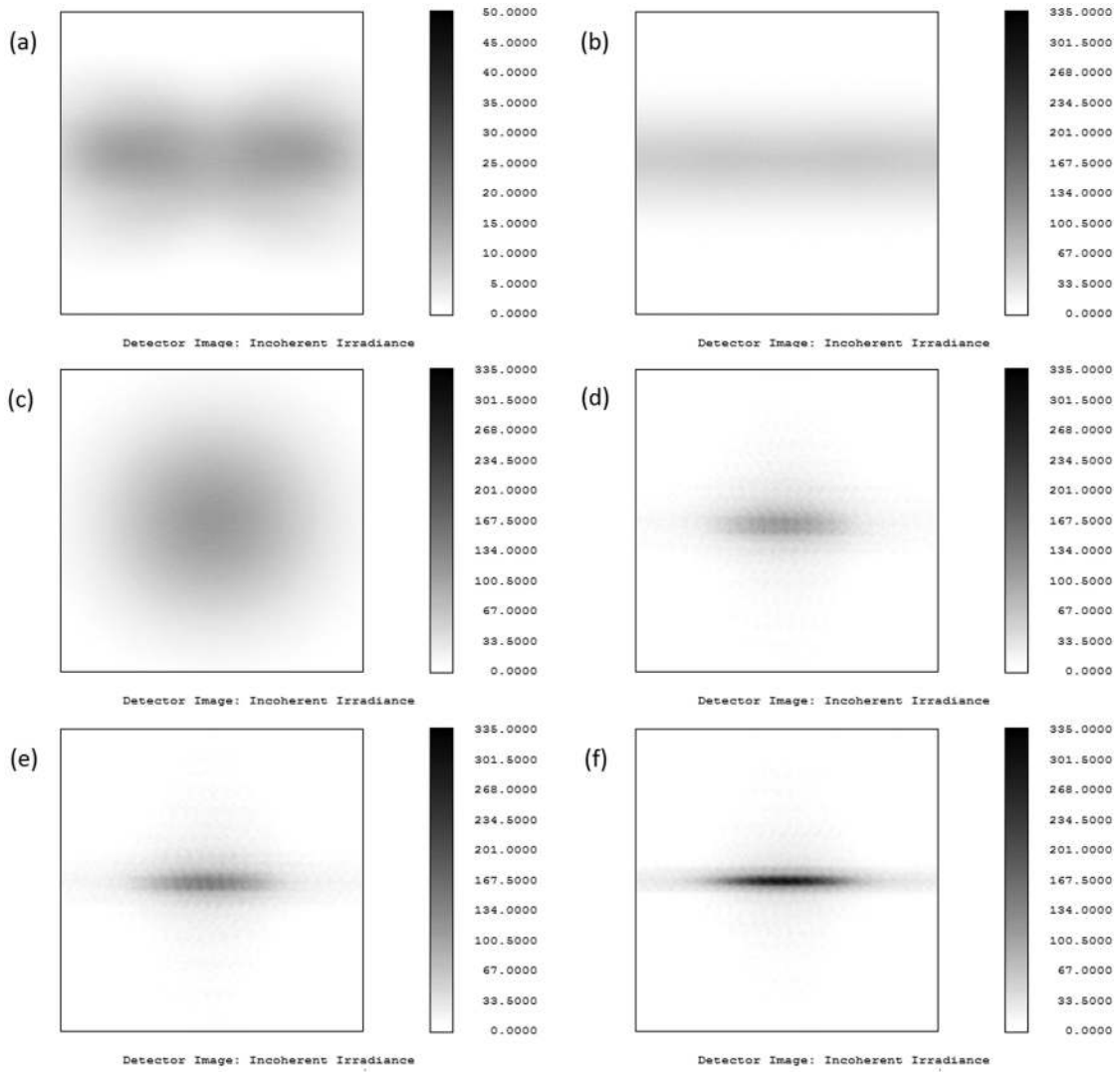

Fig. 11. Comparison of beam profiles produced by linear arrays of Duris E2 LEDs fitted with commercially available optics, with beam profiles produced by linear arrays of Duris E2 LEDs fitted with the optical system proposed in this paper. Greyscale represents incoherent irradiance (Wm^{-2}). Working distance = 1 m in all cases. (a) Detector size: 1000 × 1000 mm. (b)–(f) Detector size: 400 × 400 mm. Detector size has been varied to best display the results, as beam sizes vary depending on the optic. (Top-bottom, left-right) (a) Carclo elliptical (#10415), 10 mm diam., Max. Irradiance = 16 Wm^{-2} (b) Carclo elliptical (#10619), 20 mm diam., Max. Irradiance = 60 Wm^{-2} (c) Carclo symmetric (#10138), 20 mm diam., Max. Irradiance = 110 Wm^{-2} (d) Primary lens elements: A_n; Secondary lens: Fresnel lens (efl = 19 mm), Max. Irradiance = 110 Wm^{-2} (e) Primary lens elements: A_n; Secondary lens: Fresnel lens (efl = 25 mm), Max. Irradiance = 140 Wm^{-2} (f) Primary lens elements: A_n; Secondary lens: Fresnel lens (efl = 50 mm), Max. Irradiance = 290 Wm^{-2}. (The x and y axes are analogous to the mechanical x and y axes of the proposed optical system described in Fig. 1)).

functionality is achieved (see Fig. 2). A detailed example of a TIR design can be found in the paper by Jiang *et al*. [29].

In Figs. 11 and 12 the performance of the design presented in Section 3.1 is compared, using optical modeling, to a selection of line-lights based on this concept. TIR lenses were selected from the Carclo catalog, in both 10 mm and 20 mm diameters, and with symmetric and elliptical beam formats. The analysis was performed using the OSRAM Duris E2, which is a similarly sized LED (1.6 × 2.2 mm) to the OSRAM Mini TOPLED (1.4 × 2.2 mm). Photometric files are not provided

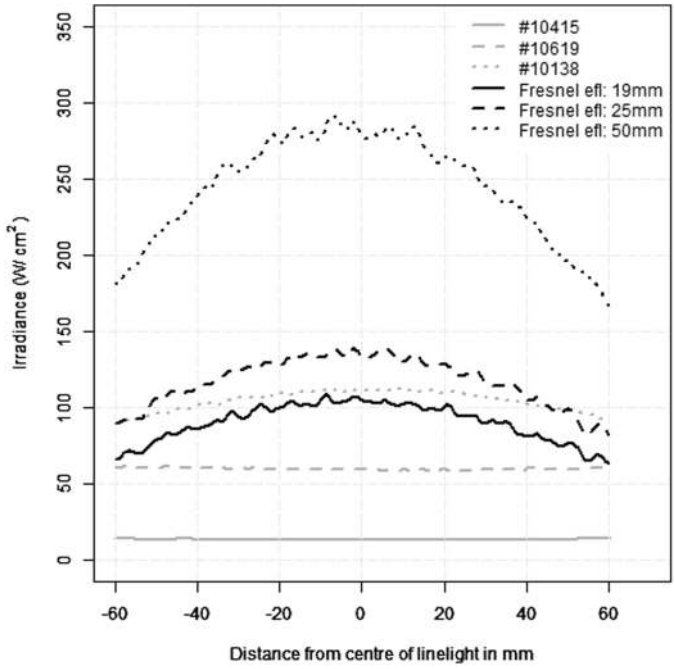

Fig. 12. Comparison of uniformity and irradiance produced by linear arrays of Duris E2 LEDs fitted with commercially available optics, with beam profiles produced by linear arrays of Duris E2 LEDs fitted with the optical system proposed in this paper. Working distance = 1 m. (a) Carclo elliptical (#10415), 10 mm diam. (b) Carclo elliptical (#10619), 20 mm diam. (c) Carclo symmetric (#10138), 20mm diam. (d) Primary lens elements: A_n; Secondary lens: Fresnel lens (efl = 19 mm) (e) Primary lens elements: A_n; Secondary lens: Fresnel lens (efl = 25 mm) (f) Primary lens elements: A_n; Secondary lens: Fresnel lens (efl = 50 mm). (The x axis is analogous/equivalent to the mechanical x axis of the proposed optical system described in Fig. 1)).

by Carclo for the OSRAM Mini TOPLED in conjunction with their lenses, but IES standardized ray files, which include the spatial and angular luminance characteristics of the source-lens system (idealized as a point source and valid in the far-field) are provided for the OSRAM Duris E2 source. The availability of such files allows simulations to be performed without having to resort to approximations, despite not having a mechanical model of the TIR, (the design of which is the protected intellectual property of the producer). These manufacturer supplied ray files were used to construct line-lights (Total array length: 120 mm i.e., 8× Duris E2 with 10 mm optics, 6× Duris E2 with 20 mm optics) with equivalent total output radiometric power (8 W) to the proposed new design described in the previous section. Scaling of LED output power was performed where appropriate, in line with manufacturer specified TIR efficiency (in the range 85–91% for all lenses used).

It can be seen that the elliptical TIRs produce low irradiance beams, with high uniformity, as they seek to spread the light in the x-axis, while confining predominantly in the y-axis. The symmetric TIRs and the proposed new design produce lower uniformity, higher irradiance beam patterns, with the 20 mm Carclo (#10138) producing a circular beam pattern with a peak irradiance of 110 Wm^{-2}, while the proposed new design produces a narrow elliptical/linear beam, with the highest peak irradiance (330 Wm^{-2}) observed for the Fresnel lens with the largest focal length (50 mm) tested. Improving light intensity improves signal to noise generally, and any machine vision system will benefit from this.

In terms of irradiance across the entire length of the beam, the proposed new design with Fresnel lenses with focal length greater than 19 mm outperforms the line-lights produced with Carclo TIRs. This data is summarized in Table 1.

TABLE 1
Summary of Optical Modeling With Linear Arrays of Carclo TIR Lens, Versus Proposed New Optical Design, Using an 8 W (radiometric power) Array of Duris E2

Design	Lens Details (Catalog # / type)	Maximum Irradiance (Wm^{-2})
Linear array of Carclo TIR lenses	Catalog #: 10415	16
	Catalog #: 10619	60
	Catalog #: 10138	110
New design (Secondary Fresnel lens + $A_1 - A_8$ primary lens elements)	19 mm Fresnel + $A_1 - A_8$ primary lenses	110
	25 mm Fresnel + $A_1 - A_8$ primary lenses	140
	50 mm Fresnel + $A_1 - A_8$ primary lenses	290

5. Conclusions

An optical system for a collimated LED line-light has been developed and tested. The design utilizes TIRs designed using an adaptation of the free-form method described by Chen *et al.* [26], coupled to a Fresnel lens which can be user selected to comply with mechanical tolerances of a specific system, while maximizing collimation. A monochromatic prototype unit was constructed, and its optical output measured at a plane 500 mm from the source, producing a highly elliptical beam, with excellent irradiance at the target plane. Further optical testing confirms good agreement between experimental performance and performance predicted via optical modeling. Using optical modeling techniques, comparison has been made to line-lights constructed using commercially available TIRs, and the new design has been found to exceed their performance, in terms of irradiance at the target plane, by up to 200% (dependent on choice of Fresnel lens).

References

[1] A. Hornberg Ed., *Handbook of Machine Vision*. Hoboken, NJ, USA: Wiley, 2006.
[2] S. X. Godber and M. Robinson, "Machine vision using line-scan sensors," *Proc. SPIE*, vol. 1823, no. 114, pp. 2–3, 1992.
[3] Teledyne DALSA, "Understanding line scan camera applications," White Paper, 2014. [Online]. Available: http://leadwise.mediadroit.com/files/292072069_TD.LineScanApp_whitepaper.v4.pdf
[4] L.-P. Zhao, X. Li, and Z.-P. Fang "TIR illumination technology for defect inspection of plastic ophthalmic lenses," *Opt. Precis. Eng.*, vol. 19, no. 9, pp. 2247–2254, 2011. http://dx.doi.org/10.3788/ope.20111909.2247
[5] N. Neogi, D. K. Mohanta, and P. K. Dutta, "Review of vision-based steel surface inspection systems," *EURASIP J. Image Video Process.*, vol. 50, pp. 2–4, 2014.
[6] A. Kumar, "Computer-vision-based fabric defect detection: A survey," *IEEE Trans. Ind. Electron.*, vol. 55, no. 1, pp. 348–363, Jan. 2008.
[7] A. K. Jain and C. Dorai, "Practicing vision: Integration, evaluation and applications," *Pattern Recognit.*, vol. 30, no. 2, pp. 183–196, 1997.
[8] C. C. Yang, K. Chao, M. S. Kim, D. E. Chan, H. L. Early, and M. Bell, "Machine vision system for on-line wholesomeness inspection of poultry carcasses," *Poultry Sci.*, vol. 89, no. 6, pp. 1252–1264, 2010.
[9] Z. Zhi-Feng *et al.*, "Research on influence on luminance of machine vision to measure cotton defects," in *Proc. Int. Conf. Optoelectron. Microelectron.*, 2015, pp. 101–103.
[10] Z. Zhang, S. Zhang, and Q. Li "Surface defects inspection method for the medium and heavy plate," *Recent Patents Mech. Eng.*, vol. 9, no. 3, pp. 255–258, 2016.
[11] L. Norton-Wayne, M. Bradshaw, and A. J. Jewell, "Machine vision inspection of web textile fabric," in *Proc. Brit. Mach. Vis. Conf.*, 1992, pp. 217–226.
[12] T. Bergin, J. Cusack, and K. DeSmet, "Advantages of LED lighting in vision inspection systems," QuadTech, Inc., White Paper, 2010. [Online]. Available: http://www.quadtechworld.com/downloads/whitepapers/wp022010.pdf

[13] H. C. Chen, J. Y. Lin, and H. Y. Chiu, "Rectangular illumination using a secondary optics with cylindrical lens for LED street light," *Opt. Exp.*, vol. 21, no. 3, pp. 3201–3212, 2013.
[14] N. Menn, *Practical Optics*. New York, NY, USA: Academic, 2004, ch. 3.
[15] M. R. Feldman, W. H. Welch, R. D. Te Kolste, and J. E. Morris, "Diffractive optics for packaging of laser diodes and fiber-optics," in *Proc. 46th Electron. Compon. Technol. Conf. Proc.*, 1996, pp. 1278–1283.
[16] I. Powell, "Linear diverging lens," U.S. Patent 4826299 A, 1989.
[17] V. Sinhoff, S. Hambuecker, K. Kleine, O. Ruebenach, and C. Wessling, "Micro-lens arrays for laser beam homogenization and transformation," *Proc. SPIE*, vol. 8605, no. 9, 2013, Art. no. 860509.
[18] I. Fujieda, T. Kosugi, and Y. Inaba, "Speckle noise evaluation and reduction of an edge-lit backlight system utilizing laser diodes and an optical fiber," *J. Display Technol.,* vol. 5, 11, pp. 414–417, 2009.
[19] P. Schreiber, S. Kudaev, P. Dannberg, and U. D. Zeitner, "Homogeneous LED-illumination using microlens arrays," *Proc. SPIE*, vol. 5942, pp. 188–1962005.
[20] X. H. Lee, I. Moreno, C. C. Sun, "High-performance LED street lighting using microlens arrays," *Opt. Exp.*, vol. 21, no. 9, pp. 10612–10621, 2013.
[21] O. Hissmann, "Web inspection in film extrusion and coating – a benefit for the producer," OCS Optical Control Systems GmbH, White Paper, 2004. [Online]. Available: http://www.tappi.org/content/enewsletters/eplace/2004/12-2Hissmann.pdf
[22] Y. Luo, Z. Feng, Y. Han, and H. Li, "Design of compact and smooth free-form optical system with uniform illuminance for LED source," *Opt. Exp.*, vol. 18, no. 9, pp. 9055–9063, 2010.
[23] Y. Ding, X. Liu, Z. R. Zheng, and P. F. Gu "Freeform LED lens for uniform illumination," *Opt. Exp.*, vol. 16, no. 17, pp. 12958–12966, 2008.
[24] M. A. Moiseev, L. L. Doskolovich, and N. L. Kazanskiy, "Design of high efficient free-form LED lens for illumination of elongated rectangular regions," *Opt. Exp.*, vol. 19, no. S3, pp. A225–A233, 2011.
[25] O. Ziemann, J. Krauser, P. Zamzow, and W. Daum, *POF Handbook: Optical Short Range Transmission Systems*. New York, NY, USA: Springer-Verlag, 2008, p. 392.
[26] J. J. Chen, T. Y. Wang, K. L. Huang, T. S. Liu, M. D. Tsai, and C. T. Lin "Freeform lens design for LED collimating illumination," *Opt. Exp.*, vol. 20, no. 10, pp. 10984–10995, 2012.
[27] R. J. Koshel, Ed., *Illumination Engineering: Design With Nonimaging Optics*. Hoboken, NJ, USA: Wiley, 2013.
[28] Zemax 13, "Optical design program," *User's Manual*, Feb. 20, 2013.
[29] J. Jiang, S. To, W. B. Lee, and B. Cheung, "Optical design of a freeform TIR lens for LED streetlight," *Optik – Int. J. Light Electron Opt.*, vol. 121, no. 19, pp. 1761–1765, 2010.